Aggelos Bletsas, Panos N. Alevizos,
and Georgios Vougioukas

The Art of Signal Processing in Backscatter Radio for μW (or Less) Internet of Things

Intelligent signal processing and backscatter radio enabling batteryless connectivity

INTERNET OF THINGS—ISTOCKPHOTO.COM/IAREMENKO
CIRCUITS—IMAGE LICENSED BY INGRAM PUBLISHING

Digital Object Identifier 10.1109/MSP.2018.2837678
Date of publication: 28 August 2018

Backscatter (or simply *scatter*) radio is based on reflection principles, where each tag modulates information on top of an illuminating signal, by simply connecting its antenna to different loads; modulation of information is based on the modifications of the tag antenna-load reflection coefficient, requiring in principle only a switch and omitting power-consuming signal conditioning units, such as mixers, amplifiers, oscillators, and filters. The ultralow-power nature of backscatter radio, in conjunction with the recent advances in multiple access and achieved communication ranges (on the order of hundreds of meters to kilometers), due to intelligent signal processing, elevate backscatter radio as the de facto communication principle for μW (or less)-level consumption, last-mile connectivity, and Internet of Things (IoT) networking. This article is an update to the state-of-the-art advances in the emerging backscatter radio domain, focusing on the signal processing engine, including ambient illumination from existing signals, as well as unconventional backscatter radio-based IoT technologies that could revolutionize environmental sensing and agriculture. Finally, the offered research methodology and techniques in short-packet, channel-encoded (or not), coherent (or not) sequence detection will assist researchers in radio-frequency identification (RFID)/backscatter radio as well as other domains of the telecommunications industry.

Introduction

RFID is based on backscatter, i.e., reflection radio, where each tag modulates information on top of an illuminating signal by simply connecting its antenna to different loads (Figure 1); modulation of information is based on the modifications of the tag antenna-load reflection coefficient, requiring in principle only a (transistor) switch and an antenna to reflect information, omitting power-consuming signal conditioning and generating units, such as mixers, amplifiers, oscillators, and filters. Thus, backscatter radio is a promising solution for ultralow-power radio communication and networks [1]. Recent work has demonstrated backscatter communication with a few

μW consumption at the tag [2]–[4] even at continuous, nonduty-cycled operation [5].

The basic limitation of passive RFIDs in terms of communication range, on the order of meters, stems from the fact that they are batteryless, harvesting their required energy from the illuminating signal; the bottleneck element has been the RF harvesting circuitry sensitivity and not the backscatter radio principle. Seminal work in [1] was the first to decouple RF harvesting from backscatter radio and showed that semipassive tags, i.e., reflection radio tags with an external power source (e.g., a coin battery) could be received by a software-defined radio (SDR) with extended communication ranges. Work in [1] highlighted the idiosyncrasies of backscatter radio, e.g., the fact that tag modulation occurs at passband; thus, orthogonal signaling, e.g., frequency-shift keying (FSK) reception using the detectors for conventional (Marconi) radio, would result in a 3-dB loss, since half of the useful signal (and appropriate matched filters) would be overlooked. Orthogonal switching signaling among multiple tags allowed for collision-free multiple access, even with a common carrier, while noncoherent, symbol-by-symbol detection of continuous phase FSK, i.e., minimum-shift keying (MSK), was demonstrated in SDR.

The need for low-complexity, resource-constrained tags, as well as the basic requirement for extended communication range, coverage, and fast, low-complexity reception, imposes additional challenging requirements in terms of nontrivial signal processing at the reader. Decoupling the illuminating emitter from the receiver of the backscattered signals (bistatic architecture) offers flexibility and better link budgets at the expense of additional channel unknowns, since emitter-to-tag and tag-to-reader links become distinct (see Figure 2). Additionally, the tag-reflected packets must be relatively short to reduce energy consumption at the tag and expedite the processing at the reader in network setups, with multiple tags operating simultaneously.

Reflector/tag: Scatter radio principles

The simplest case of backscatter radio utilizes only two passive loads: the tag/reflector modulates information by modifying the refection coefficient of the tag antenna and connected load. In that way, the induced signal at the tag antenna, stemming from a distant illuminator, is reflected back with modified amplitude and phase.

More specifically, a modified reflection coefficient is defined as $\Gamma_i = (Z_i - Z_a^*)/(Z_i + Z_a)$, where $i \in \{0,1\}$ for the two loads Z_0, Z_1 and Z_a is the (complex in general) tag antenna characteristic impedance at the utilized carrier frequency. The baseband equivalent signal, when the tag antenna is connected at load Z_i, with corresponding reflection coefficient Γ_i, $i \in \{0,1\}$, is given by

$$A_s - \Gamma_i,$$

where A_s is the (complex) load-independent tag antenna structural mode; the latter depends on the geometry and construction materials of the antenna. More than two loads and hence, multiple bits per load, have been also recently demonstrated with energy-efficient circuits [6], [7].

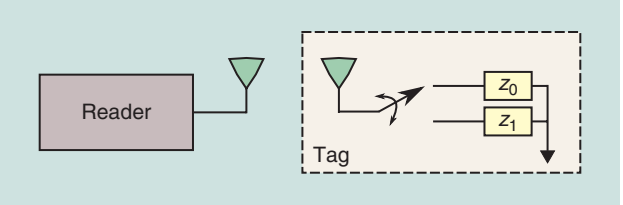

FIGURE 1. The backscatter radio principle: information is modulated on reflection at the tag of an illuminating signal, using (at least) two loads; only switching at the tag between loads is needed, omitting power-consuming signal conditioning and generating modules (e.g., amplifiers).

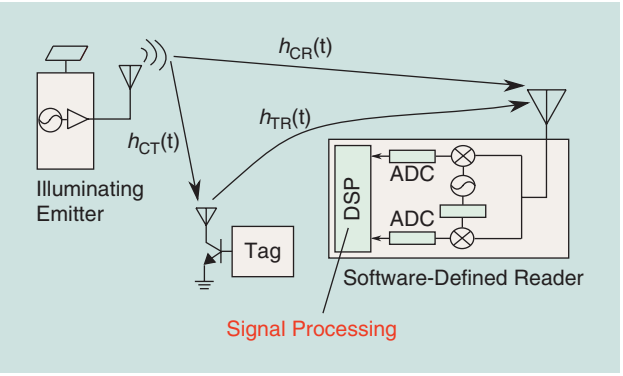

FIGURE 2. The backscatter radio principle: intelligent signal processing at the receiver allows for extended communication ranges and tag networking.

Orthogonal and nonorthogonal tag signaling

The simplest case for binary tag modulation occurs when the tag terminates its antenna at load for the whole bit duration T, i.e., at Z_0 (Γ_0) for bit "0" and Z_1 (Γ_1) for bit "1." This is the case of nonorthogonal signaling, utilized in industrial RFIDs, commonly referred to as *on-off keying* (*OOK*). Thus, assuming that $\Gamma_{\text{tag}} = \Gamma_0$ for $x_n = -1$, $\Gamma_{\text{tag}} = \Gamma_1$ for $x_n = +1$, where x_n is the (binary) information of the nth bit, the baseband equivalent of the tag-backscattered signal is given by

$$A_s - \Gamma_{\text{tag}} = \left(A_s - \frac{\Gamma_0 + \Gamma_1}{2}\right) + x_n \frac{\Gamma_0 - \Gamma_1}{2}, x_n \in \{\pm 1\}, \quad (1)$$

$$\Rightarrow x_{\text{Tag}}(t) = \left(A_s - \frac{\Gamma_0 + \Gamma_1}{2}\right) + \frac{\Gamma_0 - \Gamma_1}{2} x_n \, \Pi_T(t - nT), \quad t \in [nT, (n+1)T), \quad (2)$$

$\Pi_T(t) = 1$ for $t \in [0, T)$ and zero elsewhere.

Alternatively, the tag can continuously switch between the two loads during bit reflection, with switching frequency F_0 for bit "0" or F_1 for bit "1." This is the case of orthogonal signaling, as in FSK. If the switching pattern of the tag during the nth bit has a fundamental frequency F_0 (period $1/F_0$) for bit "0" ($x_n = -1$) and F_1 for bit "1" ($x_n = 1$), the baseband

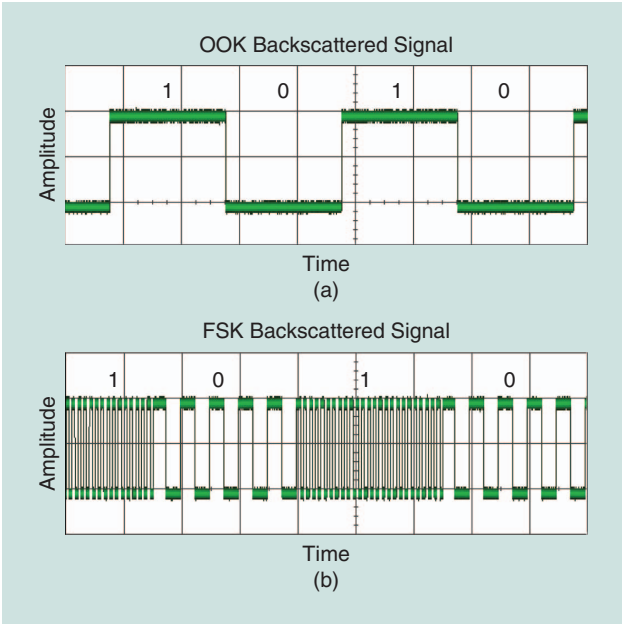

FIGURE 3. The time-domain amplitude of tag-modulated backscatter (complex) baseband signal: (a) OOK and (b) FSK.

equivalent of the tag backscattered signal for the nth binary-modulated information bit is given by

$$x_{\text{Tag}}(t) = \left(A_s - \frac{\Gamma_0 + \Gamma_1}{2}\right) + \frac{\Gamma_0 - \Gamma_1}{2} b_n(t - nT), \quad t \in [nT, (n+1)T), \tag{3}$$

where $b_n(t)$ is a (periodic) pulse train with fundamental frequency $F_{x_n} \in \{F_0, F_1\}$ and duration equal to bit duration T, with $T \gg \max(1/F_0, 1/F_1)$. Additionally, $|F_0 - F_1| = k/(2T)$ for coherent detection, and $|F_0 - F_1| = k/T$ for noncoherent detection, $k \in \mathbb{Z}$.

For $b_n(t)$ a 50% duty-cycle pulse train and even, i.e., $b_n(t) = b_n(-t)$, the following Fourier series representation holds:

$$b_n(t) = \frac{4}{\pi} \sum_{k=0}^{+\infty} \frac{1}{2k+1} \cos[2\pi(2k+1)F_{x_n} t], \tag{4}$$

i.e., only odd harmonics exist due to 50% duty cycle and only cosines, due to being even. For $b_n(t)$ a 50% duty-cycle pulse train and odd, i.e., $b_n(t) = -b_n(-t)$, the following Fourier series representation holds:

$$b_n(t) = \frac{4}{\pi} \sum_{k=0}^{+\infty} \frac{1}{2k+1} \sin[2\pi(2k+1)F_{x_n} t], \tag{5}$$

i.e., only odd harmonics exist due to 50% duty cycle and only sines, due to being odd. Thus, timing during tag modulation matters, and there is remaining phase Φ at the tag backscattered signal due to imperfect timings during tag modulation, modeled as follows:

$$b_n(t) = \frac{4}{\pi} \sum_{k=0}^{+\infty} \frac{1}{2k+1} \cos[2\pi(2k+1)F_{x_n} t + \Phi]. \tag{6}$$

The amplitude of the baseband tag-backscattered signal for OOK and FSK is shown in Figure 3(a) and (b), respectively, as measured in the laboratory. The advantage of OOK is that it is exploited in Gen2, the industrial RFID protocol, as previously mentioned; the disadvantage is that the spectrum of the tag's backscattered signal is centered at the illuminator's carrier frequency, where extensive reflections from the environment occur, offering clutter noise and limiting signal-to-noise ratio (SNR); furthermore, OOK requires time-domain multiplexing of several tags, requiring a receiver at each tag and carrier-sense multiple access; Gen2 RFIDs utilize framed Aloha. Alternatively, detecting simultaneously backscattering tags can be performed with time-domain, signal-specific techniques at the reader [8].

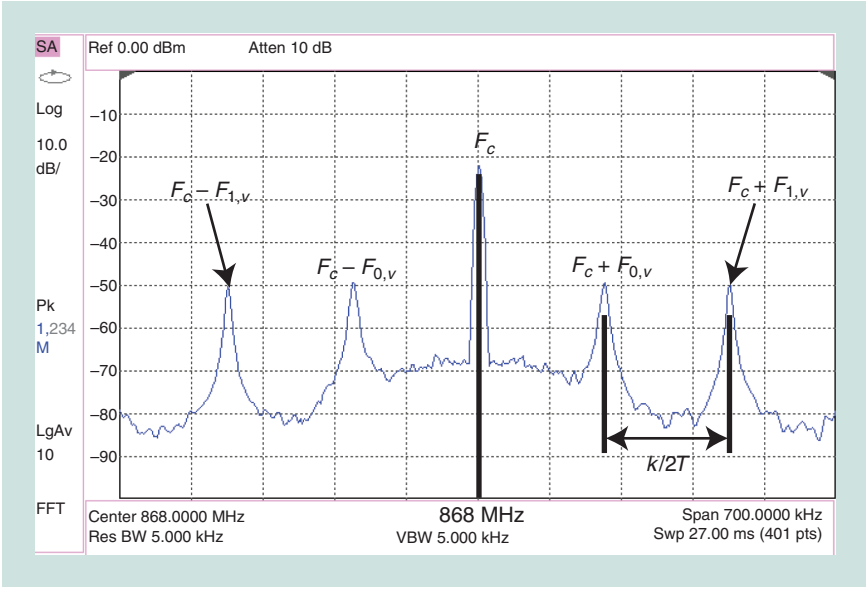

FIGURE 4. Switching between two loads with F_0 (F_1) offers at least two peaks around the illuminator's carrier frequency F_c at $F_c \pm F_0$ ($F_c \pm F_1$). Careful selection of the switching frequencies offers collision-free simultaneous backscattering from multiple tags.

Figure 4 shows a portion of measured spectrum (at the lab) for binary FSK backscattering, depicting the four peaks of the fundamental frequencies F_0, F_1 around the carrier frequency F_c of the illuminator; there are two peaks for F_0 due to the cosine term of (6) and another two for F_1; it is noted that the peaks due to the (odd) harmonics of (6) are not depicted. FSK is tailored to the power-limited regime, where backscatter operates and allows for receiverless tags, multiplexed at the frequency domain; networking several tags, simultaneously backscattering, becomes easily possible using simple

signal processing at the physical layer: all that is required is assigning distinct switching frequency pairs $\{F_{0,\nu}, F_{1,\nu}\}$ for different tags, i.e., $\nu = 1, 2, \ldots, N$ tags [1]. However, such a solution may not be applicable for a large number of high-bit-rate sensors.

This shows a fundamental difference of backscatter radio, compared to conventional Marconi radios: modulation occurs directly at the induced (at the tag) illuminator signal, without any type of upconversion at passband; thus, detection techniques should be tailored to such idiosyncrasy. For example, applying common FSK detection schemes at the signal of Figure 4 could neglect half of the peaks and, thus, half of the useful signal.

Finally, it is noted that there may be a combination of the previously described modulations; each tag can be assigned a unique switching frequency F_ν between the two loads, with a 50% duty cycle, to enjoy frequency-domain multiple access among various tags $\nu = 1, 2, \ldots$ and also exploit modifications of Φ in (6) for the transmission of information [9].

Tag pulse shaping and structural mode

Could only two tag termination loads be used to better shape the backscattered spectrum and improve spectral efficiency? For example, is there any way to alleviate the existence of odd-order harmonics in backscatter FSK, using only two loads at the tag? The answer is given in Lemma 1.

Lemma 1

Pulse shaping in backscatter radio tags with only two loads is possible [1]. Work in [1] utilized two loads and minimum shift keying (MSK), a special variant of binary FSK: instead of (6), where switching frequency changes abruptly at the bit boundaries, the tag implements MSK by continuously changing the instantaneous switching frequency (and, hence, signal phase), so that no discontinuities occur at the bit boundaries; such an operation was performed at the tag using an embedded phase-locked loop, offering power spectral density (PSD) of the backscattered signal that dropped with the fourth power of frequency, as opposed to conventional PAM/quadrature amplitude modulation/PSK (where PSD drops with the square of frequency). MSK can also be seen as offset-quadrature PSK with memory and sinusoid modulating pulses, corroborating its inherent pulse-shaping nature.

Pulse shaping with FSK and more than two loads was recently proposed in [10]: switching alternatively between a series of loads implemented a (rotating) complex phasor, multiplying the induced (at the tag) signal and, thus, shifting its spectrum only right (or left) of the illuminating carrier frequency, depending on the rotating direction. In that way, smaller bandwidth could be utilized.

Finally, it is noted that the current mind-set in backscatter literature dismisses the value of the tag antenna's structural mode. That is due to the fact that, for binary coherent (i.e., minimum distance) detection, the distance between the utilized constellation points $|(A_s - \Gamma_0) - (A_s - \Gamma_1)| = |\Gamma_1 - \Gamma_0|$ matters, which is A_s independent. However, for certain bistatic scenarios (e.g., a blocked illuminator-to-reader link) and certain housekeeping tasks before detection [e.g., carrier frequency offset (CFO) estimation], A_s matters [11]. A measurement and estimation method for A_s can be found in [12].

Universal system model: Monostatic versus bistatic versus ambient

Figure 2 depicts the case of bistatic backscatter radio, where the illuminator of the tag and reader of the tag-backscattered signal are distinct units, placed at different locations. Assuming flat fading, the channel impulse response between illuminator and reader, illuminator and tag, and tag and reader is given by $h_{\rm m}(t) = a_{\rm m}\delta(t - \tau_{\rm m})$, with ${\rm m} \in \{{\rm CR}, {\rm CT}, {\rm TR}\}$, respectively; the baseband equivalent for each link is given by $a_m e^{-j2\pi f_c \tau_m}$, where s_f is the utilized carrier frequency. Based on this modeling, the baseband representation of the received signal at the reader is given by (Figure 2)

$$\mathsf{y}(t) = a_{\rm CR}\mathsf{e}^{-{\rm j}\phi_{\rm CR}}\mathsf{c}(t) + a_{\rm CT}\mathsf{e}^{-{\rm j}\phi_{\rm CT}}a_{\rm TR}\mathsf{e}^{-{\rm j}\phi_{\rm TR}}\mathsf{s}x_{\rm Tag}^{\rm mod}(t) + \mathsf{n}(t), \tag{7}$$

where $\phi_{\rm m} = 2\pi f_c \tau_{\rm m}$, with ${\rm m} \in \{{\rm CR}, {\rm CT}, {\rm TR}\}$, $\mathsf{c}(t)$ is the signal transmitted by the illuminator, $\mathsf{n}(t)$ models white complex Gaussian noise at the reader, and s models nonidealities in backscattering efficiency at the tag (e.g., due to mismatches, imperfect estimation of load values, etc.). For bistatic setups, the illuminator transmits a simple carrier signal $\mathsf{c}(t) = \sqrt{2P_{\rm C}}\,\mathsf{e}^{-{\rm j}(2\pi\Delta F t + \Delta\phi)}$, with carrier frequency and phase offset between illuminator and reader denoted by ΔF and $\Delta\phi$, respectively, and $P_{\rm C}$ as the illuminator's transmission power; in that case, $x_{\rm Tag}^{\rm mod}(t)$ in (7) is given by $x_{\rm Tag}^{\rm mod}(t) = \sqrt{2P_{\rm C}}\,\mathsf{e}^{-{\rm j}(2\pi\Delta F t + \Delta\phi)}x_{\rm Tag}(t)$. Notice that, for monostatic systems where illuminator and reader share the same oscillator, the CFO is zero ($\Delta F = 0$) and the link carrier reader models the duplexer's imperfection, i.e., the signal leakage from the transmit to the receive chain (e.g., due to circulator's imperfection and coupling effects); the system model (7) can describe both bistatic as well as monostatic setups.

It also noted that the previously described system model can describe asymmetric scenarios, i.e., when the channel statistics between tag and reader are vastly different than the statistics between tag and illuminator; it can also describe the case of ambient illuminators, i.e., when the illuminating signal $\mathsf{c}(t)$ is already modulated; in that case, $\mathsf{c}(t) = \mathsf{m}(t)\mathsf{e}^{-{\rm j}(2\pi\Delta F t + \Delta\phi - \phi(t))}$, where $\mathsf{m}(t)\mathsf{e}^{{\rm j}\phi(t)}$ is the complex envelope of the ambient illuminator's signal. The previously mentioned bistatic model, where the illuminator was decoupled from the reader, appeared first in [11] and [13]–[15]; work in [16] and [17] studied a similar model, having in mind multiple (colocated) antennas at the reader and multiple antennas at the tag; ambient backscatter [18] is a special case of the bistatic architecture.

Due to the lack of any type of specialized filtering/signal conditioning or amplification, there is no additional noise term induced by the tag at (7). Backscatter communication is power limited, and required signal processing for reliable detection becomes challenging. Furthermore, there are many unknown

channel and tag-dependent parameters, pointing toward the direction of noncoherent processing. We will summarize breakthroughs in noncoherent, as well as coherent, processing next. Finally, for ultralow-power and low-bit-rate backscatter sensor networks, short packets must be employed to reduce computation complexity at the tag and computation and decoding complexity at the reader, especially when several streams from multiple tags are processed in parallel. We will also summarize recent findings in short-packet communication techniques that could be beneficial to other domains.

Receiver: Noncoherent processing

Symbol-by-symbol detection

Figure 5 depicts four matched filters, in the form of correlators: two for the signals that correspond to F_0 and another two for the signals that correspond to F_1 (as explained in the previous secton). The correlator is equivalent to a matched filter for perfect synchronization. Before filtering, necessary carrier frequency estimation ($\Delta\hat{F}$) using periodograms and compensation is performed (assuming bistatic setups), as well as dc offset removal (through time average removal); the outcome per bit of such filtering is a 4×1 complex vector $\mathbf{r}=[r_0^+\ r_0^-\ r_1^+\ r_1^-]^\top$; work in [11] and [13]–[15] suggested the following energy-based, noncoherent detector:

$$\left|r_0^+\right|^2+\left|r_0^-\right|^2 \overset{\text{bit }0}{\geq} \left|r_1^+\right|^2+\left|r_1^-\right|^2. \tag{8}$$

An immediate question arises: Why is squaring of the amplitudes in (8) required and not simply taking the absolute norm? The answer is provided next.

Subsequent work proved that (8) is the outcome of hybrid composite hypothesis testing (HCHT) symbol-by-symbol detection. Denoting $\mathbb{B}\equiv\{0,1\}$, $\mathbf{s}_i=[1-i\ 1-i\ i\ i]^\top$, $i\in\{0,1\}$, Φ_0 and Φ_1 the value of Φ in (6), for bit "0," bit "1," respectively, $\mathbf{\Phi}=\{\Phi_0,\Phi_1\}$,

$$\mathrm{E}=\kappa^2 P_C\left|\Gamma_0-\Gamma_1\right|^2 s^2 T,\ h=a_{CT}\,a_{TR}\,e^{j(\phi_{CT}+\phi_{TR}+\Delta\phi+\angle(\Gamma_0-\Gamma_1))}, \tag{9}$$

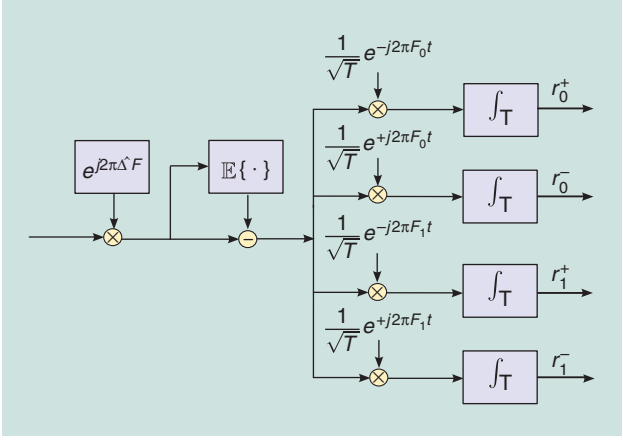

FIGURE 5. Backscatter FSK, as described by (6) and (7), requires four matched filters, not two.

and $\mathrm{x}_i(\mathbf{\Phi})=\sqrt{\frac{\mathrm{E}}{2}}\left[\mathrm{e}^{+\mathrm{j}\Phi_0},\mathrm{e}^{-\mathrm{j}\Phi_0},\mathrm{e}^{+\mathrm{j}\Phi_1},\mathrm{e}^{-\mathrm{j}\Phi_1}\right]^\top\odot\mathbf{s}_i$, $i\in\mathbb{B}$, where $\odot$ denotes point-wise multiplication and κ is a constant, Theorem 1 is presented, assuming complex white Gaussian noise at the receiver [19], [20].

Theorem 1: Noncoherent HCHT symbol-by-symbol backscatter FSK detection

$$\arg\max_{i\in\mathbb{B}}\left\{\mathbb{E}_{\mathbf{\Phi}}\left[\max_{h\in\mathbb{C}}\ln\left[\mathrm{f}(\mathbf{r}\,|\,i,h,\mathbf{\Phi})\right]\right]\right\}$$
$$\Leftrightarrow\left|r_0^+\right|^2+\left|r_0^-\right|^2\underset{i=1}{\overset{i=0}{\gtrless}}\left|r_1^+\right|^2+\left|r_1^-\right|^2, \tag{10}$$

where $\mathrm{f}(\cdot\,|\,\cdot)$ denotes the conditional pdf; the expectation operation (10) gets rid of the unknown phases $\mathbf{\Phi}$, while the maximization operator offers estimation of the unknown channel (and, hence, the hybrid nature of the detector). Interestingly, a pure maximization operation for both unknowns, i.e., a generalized likelihood ratio test (GLRT) receiver, offers the result given in Theorem 2 [19], [20].

Theorem 2: Noncoherent GLRT symbol-by-symbol backscatter FSK detection

$$\arg\max_{i\in\mathbb{B}}\left\{\max_{\mathbf{\Phi}\in[0,2\pi)^2}\max_{h\in\mathbb{C}}\ln\left[\mathrm{f}(\mathbf{r}\,|\,i,h,\mathbf{\Phi})\right]\right\}$$
$$\Leftrightarrow\left|r_0^+\right|+\left|r_0^-\right|\underset{i=1}{\overset{i=0}{\gtrless}}\left|r_1^+\right|+\left|r_1^-\right|. \tag{11}$$

Work in [1] offered noncoherent symbol-by-symbol detection for backscatter MSK, while work in [11] and [13]–[15] also studied the case of noncoherent symbol-by-symbol for OOK, using energy-based sufficient statistics compared to carefully selected thresholds.

Short-packet/sequence detection—no channel coding

For relatively static environments, channel coherence time can be greater than packet duration, especially when packets are relatively short. Under this assumption, and denoting tag (reflected) information sequence as $\mathbf{i}=[i_1\,i_2\ldots i_{N_s}]^\top\in\mathbb{B}^{N_s}$, with $N_s\leq N_{coh}$ where $N_{coh}\in\mathbb{N}$ the channel coherence time measured in number of bit periods, and reader received sequence as $\mathbf{r}_{1:N_s}$, the GLRT sequence detector, assuming complex Gaussian noise at the receiver, is given as follows [21], [22]:

$$\mathbf{i}_{\mathrm{GLRT}}=\arg\max_{\mathbf{i}\in\mathbb{B}^{N_s}}\max_{\mathbf{\Phi}\in[0,2\pi)^2}\max_{h\in\mathbb{C}}\ln\left[\mathrm{f}(\mathbf{r}_{1:N_s}\,|\,\mathbf{i},h,\mathbf{\Phi})\right], \tag{12}$$

where $\mathrm{f}(\cdot\,|\,\cdot)$ denotes the conditional pdf; the above detector, implemented through exhaustive search, requires assessing 2^{N_s} possible sequences; such search, even for moderate sequence length N_s is prohibitive. Fortunately, Theorem 3 unlocks the GLRT potential [20], [21], [22].

Theorem 3

There exists algorithm that finds $\mathbf{i}_{\mathrm{GLRT}}$ with complexity $O(N_s\log N_s)$, instead of $O(2^{N_s})$. The algorithm provided in [20]–[22] can be applied to any orthogonal signaling, including FSK for backscatter, as well as Marconi radios; given that

orthogonal signaling is tailored to the power-limited regime, the applicability of Theorem 3 is wide, for various scenarios in flat fading, terrestrial, underwater, or satellite communications, with channel unchanged during packet/sequence transmission.

For relatively static environments, channel coherence time can be greater than packet duration, especially when packets are relatively short.

FM0 line coding, utilized in industrial (Gen2) RFID, can be seen as orthogonal signaling despite the fact that industrial RFIDs utilize OOK and not FSK. Such interpretation is possible, by observing half-bit before and half-bit after the OOK-modulated/FM0-encoded bit of interest (totaling $2T$ interval for bit duration of T). Thus, Theorem 3 offers noncoherent sequence detection of Gen2/FM0 RFID tags with loglinear complexity in the sequence length and GLRT performance, without utilizing any type of preambles.

Short-packet/sequence detection with channel coding

Relaxing the small delay requirement, interleaving of depth D can be exploited to diminish long bursts of fading while offering reliable communication in a noncoherent fashion. Assuming N_c coded bits per tag-backscattered sequence, interleaving of depth D means that the tag buffers exactly D coded sequences (of length N_c each) and backscatters them column-wise; the reader performs buffering and performs the reverse operation. Following the equivalent FSK signal model found in [23], work in [19] and [20] showed that interleaving for backscatter FSK offers the following:

$$\mathbf{r}_{1:N_c} = \begin{bmatrix} \mathbf{r}_1 \\ \mathbf{r}_2 \\ \vdots \\ \mathbf{r}_{N_c} \end{bmatrix} = \begin{bmatrix} h_1 \mathbf{x}_{c_1}(\boldsymbol{\Phi}) \\ h_2 \mathbf{x}_{c_2}(\boldsymbol{\Phi}) \\ \vdots \\ h_{N_c} \mathbf{x}_{c_{N_c}}(\boldsymbol{\Phi}) \end{bmatrix} + \begin{bmatrix} \mathbf{n}_1 \\ \mathbf{n}_2 \\ \vdots \\ \mathbf{n}_{N_c} \end{bmatrix}, \tag{13}$$

where $\mathbf{n}_i, i \in \{1,2,\ldots,N_c\}$ is a 4×1 complex, circularly symmetric Gaussian vector (with such vectors independent for distinct indexes) and the rest of notation is as in the previous sections. For $DT \geq T_{\text{coh}}$, interleaving is comparable to compound channel coefficients $\{h_i\}$ being independent for different $i \in \{1,2,\ldots,N_c\}$. Thus, the backscattered bits in a specific coded sequence/short packet enjoy statistically independent fading coefficients. Theorem 4 offers soft-decision metrics for noncoherent, channel-coded sequence detection in a structured way [19], [20].

Theorem 4

For $DT \geq T_{\text{coh}}$, noncoherent HCHT soft-decision decoding for channel-coded backscatter FSK amounts to

$$\arg\max_{\mathbf{c}\in C} \left\{ \mathbb{E}_{\boldsymbol{\Phi}} \left[\max_{\mathbf{h}\in\mathbb{C}^{N_c}} \ln[\mathsf{f}(\mathbf{r}_{1:N_c} | \mathbf{c}, \mathbf{h}, \boldsymbol{\Phi})] \right] \right\} \Leftrightarrow \arg\max_{\mathbf{c}\in C} \sum_{n=1}^{N_c} w_n c_n, \tag{14}$$

where $w_n \triangleq |r_1^+(n)|^2 + |r_1^-(n)|^2 - \left(|r_0^+(n)|^2 + |r_0^-(n)|^2 \right)$, $n = 1, 2, \ldots, N_c$, $\mathbf{h} = [h_1\ h_2 \ldots h_{N_c}]$, and $c_n \in \{0,1\}$.

This allows simple calculation of the most appropriate sequence among all possible coded sequences (denoted as set C). For example, there are 2^{16} possible coded sequences for a 1/2-rate code with sequence length $N_c = 32$. For small packets/coded sequences, as targeted in this work, such exhaustive search with the aforementioned weights is feasible. Other selection of weights is also possible [24]. Experimental results with Bose–Chaudhuri–Hocquenghem (BCH) and Reed–Muller (RM) codes, ultralow-cost, 8-b, microcontroller-based tags and an SDR-based reader can be found in [19], [20], and [24].

Receiver: Coherent processing

Short-packet/sequence detection with/without coding

Work in [23] offered a simplified baseband signal representation for backscatter FSK per bit [23, Th. 1]:

$$\mathbf{r} = [r_0^+\ r_0^-\ r_1^+\ r_1^-]^\top = h\sqrt{\frac{\mathrm{E}}{2}}[\mathrm{e}^{+\mathrm{j}\Phi_0}\ \mathrm{e}^{-\mathrm{j}\Phi_0}\ \mathrm{e}^{+\mathrm{j}\Phi_1}\ \mathrm{e}^{-\mathrm{j}\Phi_1}]^\top \odot \mathbf{s}_i + \mathbf{n}, \tag{15}$$

where the notation follows as in the section "Symbol-by-Symbol Detection," e.g., $\mathbf{s}_i = [1\ -i\ \ 1\ -i\ i\ i]^\top$, $i \in \{0,1\}$.

When the tag reflects a known (to the reader) preamble, the reader can find out the estimate

$$\hat{\mathbf{h}} = [\hat{h}_1\ \hat{h}_2\ \hat{h}_3\ \hat{h}_4]^\top$$

of $\mathbf{h} = h\sqrt{\frac{\mathrm{E}}{2}}[\mathrm{e}^{+\mathrm{j}\Phi_0}\ \mathrm{e}^{-\mathrm{j}\Phi_0}\ \mathrm{e}^{+\mathrm{j}\Phi_1}\ \mathrm{e}^{-\mathrm{j}\Phi_1}]^\top$ using standard least-square techniques. Thus, the coherent maximum likelihood (ML) symbol-by-symbol detector is given by

$$b_i^{\text{ML}} = \arg\max_{b_i\in\{0,1\}} \exp\left\{ -\left\| \mathbf{r} - \hat{\mathbf{h}} \odot \mathbf{s}_{b_i} \right\|^2 \right\} \Leftrightarrow \tag{16}$$

$$\mathcal{R}e((\hat{h}_1)^* r_0^+ + (\hat{h}_2)^* r_0^-) \overset{\text{bit } 0}{\geq} \mathcal{R}e((\hat{h}_3)^* r_1^+ + (\hat{h}_4)^* r_1^-), \tag{17}$$

where $\mathcal{R}e(\cdot)$ stands for the real part. Equation (17) can be easily modified to offer ML coherent decoding; the latter was tested with RM and BCH channel-encoded sequences, both in simulation, as well as experimental setups [25].

As previously mentioned in the section "Short-Packet/Sequence Detection–No Channel Coding," FM0 line coding, utilized in industrial (Gen2) RFID, can be seen as orthogonal signaling, despite the fact that industrial RFIDs utilize OOK and not FSK. Work in [26] exploited this interpretation, in conjunction with the 6-bit preambles already present in Gen2, estimated the channel, and performed optimal coherent detection with orthogonal signaling. Signal processing software for a GNU radio-based SDR receiver for Gen2/FM0 RFIDs was also open sourced.

Partially coherent detection

When all wireless channel-specific parameters are unknown but the receiver only has partial information regarding the tag-modulating phases Φ_0, Φ_1, the following partially coherent detector for backscatter FSK is possible [9]:

$$|r_0^+ + e^{2j\Phi_0} r_0^-| \overset{\text{bit } 0}{\geq} |r_1^+ + e^{2j\Phi_1} r_1^+|, \tag{18}$$

where $\mathbf{r} = [r_0^+ \; r_0^- \; r_1^+ \; r_1^-]^\top$ is defined as before and the receiver must know the tag-dependent, modulating phases Φ_0 and Φ_1; notice that this detector is different than the fully noncoherent square-law detector, described in the section "Symbol-by-Symbol Detection." Performance of the detector in (18) is given later in the section "Architectures and Network Applications."

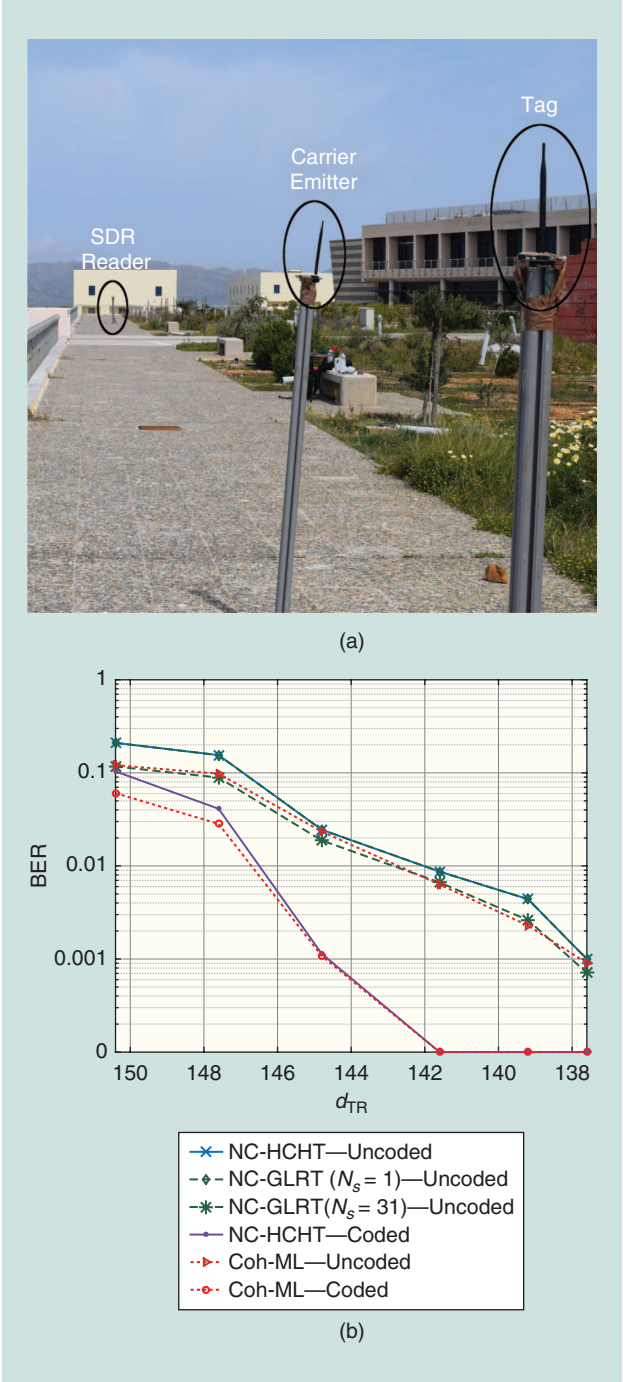

FIGURE 6. (a) and (b) Intelligent signal processing with SDR, even with a noisy receiver, has been experimentally tested, with extended tag-to-reader (d_{TR}) distances. Parameters for the figure plot include $P_t = 13$ dBm, receiver NF $\in [7 - 12]$ dB, illuminator-to-tag distance $d_{CT} = 8$ m, $T = 1$ ms, $F_1 = 2F_0 = 250$ kHz, and 16 training (preamble) + 31 data-coded bits [20].

Comparison of coherent versus noncoherent short-packet detection

The major disadvantage of coherent communication is the utilization of preamble bits at the packet, a priori known at the reader, for channel estimation. In short-packet communication, e.g., with packet payload of only 32 channel-coded bits, a preamble of 8–16 bits is comparable to the payload, requiring comparable energy, deceasing the rate, and suggests inefficient communications. For batteryless tags, where every minuscule amount of power matters, such inefficiency is further amplified.

Work in [19] studied low-bit-rate backscatter FSK communication, comparing noncoherent HCHT versus coherent ML symbol-by-symbol detection, for small packets (on the order of 100 bits), under fixed energy per packet at both cases, i.e., taking into account the energy utilized for preamble bits (in the coherent case) in packet energy budget; no fading (AWGN), Rice and Rayleigh fading were studied. It was found that the BER performance gap between noncoherent and coherent was on the order of 1 dB or less, with decreasing value when going from Rayleigh to Rice to AWGN, i.e., from a more random to a more deterministic channel.

Experimental results in [20] with both symbol-by-symbol or sequence detection, using noncoherent or coherent techniques (including BCH and RM channel coding), as described in this work, corroborated such a (perhaps major) finding: noncoherent detection can be as good as coherent (Figure 6), boosting tag-to-reader communication distances, even with high noise-figure (NF) radios. For the case of noncoherent detection, synchronization was performed without any type of pilots/preambles, solely based on energy techniques.

A note on embedded receivers

In bistatic setups, highly sensitive, conventional (Marconi), embedded receivers can be utilized for backscatter radio reception. In that case, the tag must transmit the necessary protocol bits before (and after) payload that the embedded receiver is expecting. Given that radio sensitivity depends on communication bandwidth (with higher bandwidth resulting in lower sensitivity), NF, temperature of operation, and detection method and required minimum SNR, embedded receivers with small NF and small bandwidth can, in principle, detect signals with power below –100 dBm.

Examples of backscatter bistatic radio reception using embedded FSK radios include work in [27], where Bluetooth Low Energy (BLE)-embedded modules were utilized. Another recent example is offered in [28], where backscatter bistatic FSK was received by SI1064 or TI CC1101 embedded radios, with transmit power + 13 dBm at the illuminator and illuminator-to-tag, tag-to-embedded receiver distances at 3 m and 268 m, respectively, at packet error rate (PER) of 10.6% (Figure 7), or illuminator-to-tag, tag-to-embedded receiver distances at 3 m and 246 m, respectively,

at ~1% PER. Subsequent work with LORA embedded receivers offered additional ranges with 20-dB additional illuminator transmission power and about 30-dB higher sensitivity (due to smaller bandwidth), compared to [28]. Note that 100 times smaller reception bandwidth results in 20-dB higher radio sensitivity.

Extensions to ambient environments

Theoretical studies

In [29], ambient backscatter communication is studied from an information-theoretic point of view. The setup includes an orthogonal frequency-division multiplexing (OFDM) ambient illuminator, the backscatter tag, and a legacy receiver for the illuminating signal; a dedicated receiver for the backscattered signal is considered as part of a second setup. Interestingly, it is shown that the additional paths created from the tag's backscattering may offer a performance gain for the legacy receiver.

In [30], differential modulation in conjunction with OOK is employed at the tag, while the ambient illuminator's complex baseband samples are considered to follow complex normal distribution; 8-PSK illumination is studied as well. Utilizing the signal model $y[n] = h_{CR}\mathbf{c}[n] + h_{CT}h_{TR}\mathbf{s}B[n]\mathbf{c}[n] + w[n]$ [which follows (7)], where $\mathbf{c}[n]$ denotes the ambient carriers' complex samples s.t. $\mathbf{c}[n] \sim \mathcal{CN}(0, P_s)$, $B[n] \in \{0, 1\}$, the differentially encoded tag's signal, and $w[n] \sim \mathcal{CN}(0, N_w)$ additive noise, the following two hypotheses are formed:

$$y[n] = \begin{cases} \mathcal{CN}(0, \sigma_0^2), & B[n] = 0 \\ \mathcal{CN}(0, \sigma_1^2), & B[n] = 1, \end{cases} \tag{19}$$

where $\sigma_0^2 = |h_{CR}|^2 P_s + N_w$, $\sigma_1^2 = |h_{CR} + h_{CT}h_{TR}\mathbf{s}|^2 P_s + N_w$. Based on the two hypotheses, ML (based on the aforementioned signal model) and energy-based (based on summing $|y[n]|^2$ over the duration of a single bit and comparing with a threshold) detectors were derived. Both detectors required knowledge of ambient illuminator-and channel-related parameters σ_0^2, σ_1^2, acquired in a blind way with variance estimation. However, in the aforementioned detection method, a received sequence of the next/previous $M-1$ symbols is needed before detecting symbol M, with all channel-related parameters assumed unchanged for M bit periods. Using blind estimation, complex normal illumination and energy-based detection, BER of $\simeq 8 \cdot 10^{-3}$ was achieved at transmit (based on the ambient illuminator's power) SNR of 20 dB, complementing related work in [31]. Using a similar methodology, the authors in [32] omitted the differential encoding and employed a short training sequence to assist the blind estimation method, suggesting partially coherent detection. In [33], the repeating structure of an ambient OFDM carrier, due to the presence of cyclic prefix and the channel's effect, was exploited to derive an ML detector for a single antenna receiver; multiantenna receiver design was also studied. Modeling the ambient illuminator baseband signal as a complex Gaussian ignores the modulation format of the ambient signal; furthermore, performance of tag-backscattered signal detection on top of an ambient modulated carrier should take into account realistic channel conditions, transmission power, and link budgets.

Work in [34] considers a cognitive radio network (CRN) where the secondary system's transmitter (ST) is able to

1) utilize ambient backscatter under illumination from a primary transmitter (PT) toward a secondary receiver (SR)
2) harvest energy from PT transmissions
3) communicate with an SR using active radio powered by the harvested energy.

The authors, study both underlay (the primary channel is always busy) and overlay scenarios. Optimal (with respect to secondary rate) tradeoffs regarding time allocation between backscattering and energy harvesting are presented. For the underlay case, the rate optimization problem includes the constraint of maximum allowable ST transmission power to avoid interference toward the primary channel. All of the aforementioned are recent example efforts in this exciting, rapidly evolving field [35]. A contemporary survey can be found in [36].

Practical implementations

Implementation of an ambient backscatter communication system can be found in [18], where the authors exploited

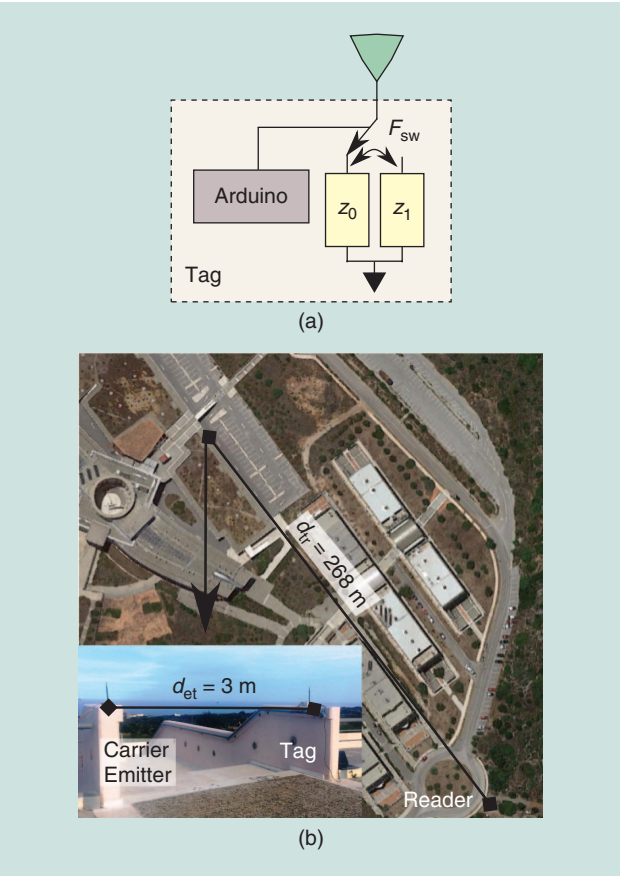

FIGURE 7. (a) A simple backscatter radio tag. (b) An experimental setup with an embedded radio receiver and illuminator-to-tag (d_{et}) and tag-to-embedded receiver (d_{tr}) distances at 3 m and 268 m, respectively [28].

illumination from ambient DTV signals and envelope detection/averaging to achieve tag-to-tag communication with range on the order of 60 cm. In [37], the authors exploited spread spectrum techniques, implemented in an analog, low-power fashion, to extend the range of tag-to-tag communication to (indicatively) 6 m for an impinged power of –15 dBm and bit rate of 3.3 bits/s, under illumination from DTV. In a similar manner, multiantenna analog design offered rates up to 1 Megabit/s with a communication range of 2 m, exploiting an impinged DTV power of –10 dBm.

Work in [38] exploited illumination from ambient FM radio signals, and the communication range (tag-to-FM receiver) was increased to approximately 18 m. Digital (audio 2-FSK, audio 4-FSK) as well analog (audio) communication was achieved. The tag was implemented using a function generator and a computer, while an integrated complementary metal–oxide–semiconductor (CMOS) design, implementing the functionality of the previous setup, was simulated. The same methodology was independently reported in [5], additionally providing a full prototype implementation [Figure 8(c)], consuming only 24 μW in continuous, nonduty-cycle operation and achieving a tag-to-receiver range of 26 m by exploiting selection diversity among various FM broadcasters; such selection diversity is easy to implement since the tag modulates directly at passband, and, thus, all FM broadcasting stations impinging on the tag antenna can be in principle exploited.

The latter two works previously mentioned demonstrate that an appropriate switching method, implemented at the tag, can result in minimum signal processing requirements at the reader side. Specifically, assume that the tag is illuminated by a FM-modulated signal, described as follows:

$$\mathrm{c}(t) = A_c \cos\left(2\pi F_c t + 2\pi k_s \int_0^t \phi(\tau)d\tau\right), \tag{20}$$

where A_c is the carrier's amplitude, F_c is the carrier's center frequency, and $\phi(t)$ is the station's information (e.g., music). The tag RF switch is driven by an FM-modulated signal $\mathrm{x}_{\mathrm{sw,FM}}(t) = A_{\mathrm{sw}} \cos\left(2\pi F_{\mathrm{sw}} t + 2\pi k_{\mathrm{sw}} \int_0^t \mu(\tau)d\tau\right)$, where $\mu(t)$ is the tag information (e.g., from a sensor). As stated in the section "Universal System Model: Monostatic Versus Bistatic Versus Ambient," the backscattered signal (ignoring microwave-related parameters, noise, and fading terms for ease of explanation) takes the following form:

$$\begin{aligned} y_{\mathrm{bs}}(t) &= \mathrm{s}\mathrm{c}(t)\mathrm{x}_{\mathrm{sw,FM}}(t) \\ &= \frac{\gamma_s}{2}\cos(2\pi(F_c + F_{\mathrm{sw}})t + \Phi_s(t) + \Phi_{\mathrm{tag}}(t)) \\ &\quad + \frac{\gamma_s}{2}\cos(2\pi(F_c - F_{\mathrm{sw}})t + \Phi_s(t) - \Phi_{\mathrm{tag}}(t)), \end{aligned} \tag{21}$$

where $\gamma_s = \mathrm{s}\, A_c\, A_{\mathrm{sw}}$, $\Phi_s(t) = 2\pi k_s \int_0^t \phi(\tau)d\tau$ and $\Phi_{\mathrm{tag}}(t) = 2\pi k_{\mathrm{sw}} \int_0^t \mu(\tau)d\tau$. Equation (21) demonstrates that if the tag is

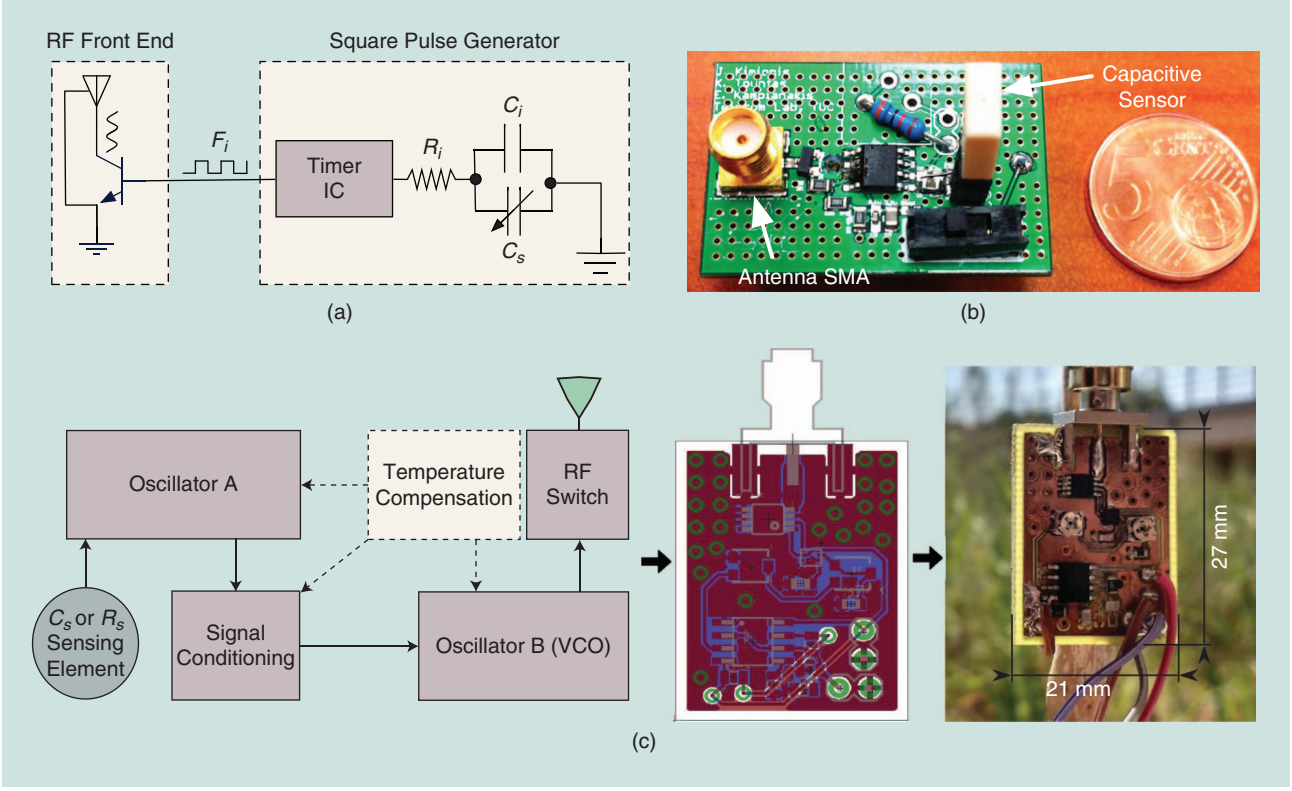

FIGURE 8. Ultralow-power backscatter radio tags: (a) and (b) environmental humidity [2]. (c) The resistive/capacitive sensor for ambient FM [5]. VCO: variable-control oscillator.

illuminated by an FM-modulated signal $\mathsf{c}(t)$ and the signal driving the RF switch is FM modulated as well (e.g., a square wave whose fundamental frequency is modulated according to the value of a sensor), then the backscattering operation results in two new FM-modulated signals, each centered at $F_s \pm F_{\text{sw}}$. Thus, any receiver capable of performing FM demodulation can recover tag/sensors' signal $\mu(t)$ with, however, interference from illuminating stations' $\phi(t)$. Additionally, if $\mu(t)$ is limited in the audible frequency range, any conventional FM broadcast receiver, including modern smartphones, can recover $\mu(t)$. Using a method similar to [18], work in [39] also exploited ambient FM illumination, achieving ranges on the order of 5 m while consuming 1.78 mW for a bit rate of 1 kb/s in duty-cycled operation. Finally, Wi-Fi-based, ambient backscatter implementations can be found in [40]–[42].

Exploiting different illuminating signals involves different tradeoffs, depending on the ambient signal modulation, the technique used at the tag to remodulate information, and the receiver architecture. For example, exploiting TV signals in [18] required envelope detection, at the expense of limited communication ranges. In contrast, exploiting FM signals [5], [38] allowed for recovery of the backscattered information by any conventional FM receiver, while providing extended ranges and means for frequency-based multiuser communication, at the expense of more complicated (but widely available) FM signal demodulation.

Architectures and network applications

Monostatic versus bistatic/multistatic architectures

In certain applications, there is great need to maximize reliability and coverage. Thus, it is important to have a concrete network design principle, tailored to backscatter radio. More specifically, is it better to adopt a monostatic architecture, where illuminator and reader antenna are the same? Or is it better to adopt a bistatic architecture, where reader and illuminator are separated units, distant in space?

It turns out that, in terms of link budget, i.e., large-scale path loss, the inherent asymmetry of the bistatic architecture helps and the bistatic outperforms the monostatic architecture; assuming free-space loss (where the received power drops with the squared distance), fixed illuminator-to-reader distance $\mathsf{d}_{\max}$ and denote as x the illuminator-to-tag distance; it can be easily seen that the average received power at the reader is proportional to

$$y(x) = \left(\frac{1}{x}\right)^2 \left(\frac{1}{\mathsf{d}_{\max} - x}\right)^2,$$

which is minimized for $x = \mathsf{d}_{\max}/2$, i.e., when the tag is equidistant from the illuminator and reader antenna, which is the case in the monostatic architecture.

It also turns out that the bistatic architecture outperforms the monostatic (where, in the latter, a common antenna for transmit and receive is assumed) in terms of small-scale loss, i.e., fading-relevant metrics, such as diversity order. The following theorems state formally the elements highlighted previously, further assuming fading amplitude distributed according to Nakagami, with normalized (equal to one) average squared value [9]:

Theorem 5

Under Nakagami fading, the BER of monostatic architecture (illuminator and reader share the same antenna) with ML coherent detection of backscatter FSK is bounded as follows:

$$\mathbb{P}(e_{l,n}^{[\text{m}]}) \le \frac{1}{2}\left(\frac{\mathtt{M}_n + \mathtt{M}_n^2}{2\,\mathtt{SNR}_n^{[\text{m}]}}\right)^{\frac{\mathtt{M}_n}{2}} \mathsf{U}\left(\frac{\mathtt{M}_n}{2}, \frac{1}{2}, \frac{\mathtt{M}_n + \mathtt{M}_n^2}{2\,\mathtt{SNR}_n^{[\text{m}]}}\right), \quad (22)$$

where $\mathtt{M}_n$ is the Nakagami parameter for link TR, $\mathsf{U}(\cdot,\cdot,\cdot)$ is given in [10, eq. (13.4.4)], and $\mathtt{SNR}_n^{[\text{m}]}$ is the average received SNR for monostatic system. For Rayleigh fading ($\mathtt{M}_n = 1$), the diversity order is 1/2.

The BER bound (22) coincides with the performance of partially coherent envelope monostatic backscatter FSK detector of (18).

Theorem 6

Under dyadic Nakagami fading, the BER of a bistatic architecture (illuminator and reader are distinct units with different antennas, and respective links with tag are independent) with ML coherent detection of backscatter FSK is bounded as follows:

$$\mathbb{P}(e_{l,n}^{[\text{b}]}) \le \frac{1}{2}\left(\frac{2\mathtt{M}_{ln}\mathtt{M}_n}{\mathtt{SNR}_{l,n}^{[\text{b}]}}\right)^{\mathtt{M}_n} \mathsf{U}\left(\mathtt{M}_n, 1 + \mathtt{M}_n - \mathtt{M}_{ln}, \frac{2\mathtt{M}_{ln}\mathtt{M}_n}{\mathtt{SNR}_{l,n}^{[\text{b}]}}\right), \quad (23)$$

where $\mathtt{M}_n$ and $\mathtt{M}_{ln}$ are the Nakagami parameters for links TR and CT, respectively, while $\mathtt{SNR}_{l,n}^{[\text{b}]}$ is the average received SNR for bistatic system. Under dyadic Rayleigh fading ($\mathtt{M}_n = \mathtt{M}_{ln} = 1$), the diversity order is one.

The previous BER bound (23) coincides with the performance of the partially coherent envelope bistatic backscatter FSK detector of (18).

Theorems 5 and 6 show that the diversity order of the bistatic architecture (for Rayleigh fading) is twice that of the monostatic, due to the independence between illuminator-to-tag and tag-to-reader links, contrary to the monostatic case. Furthermore, Theorems 5 and 6 quantify BER for both noncoherent as well as coherent backscatter FSK; it can be shown that the bistatic achitecture prevails [9]. That finding also suggests that using more than one illuminator, i.e., extending bistatic to multistatic architectures, would be highly beneficial.

In fact, a proof-of-concept, digital, multistatic backscatter radio wireless sensor network (WSN) with a single receiver, four low-cost emitters, and multiple ambiently powered, low-bit-rate tags, perhaps the first of its kind, was experimentally demonstrated in [9]. The illuminators utilized only 13-dBm transmission power in a TDMA fashion, covering an outdoor area of $3{,}500\ \text{m}^2$. Proof-of-concept, analog multistatic backscatter radio WSN with a single receiver and two low-cost emitters was presented in [2] for greenhouse environmental humidity sensing; more details are given next.

Backscatter wireless sensor networks

In the context of environmental sensing, backscatter networks have been developed for monitoring both environmental humidity and soil moisture. Work in [2] utilized analog backscatter principles based on (backscatter) FM modulation, with tags consuming 220–500 μW, while offering a root mean squared (RMS) error of 2% relative humidity, at ultralow cost (~3 Euro) per tag. The tags' implementation was based on capacitive sensing principles, where a change in a sensing capacitors' value, due to a variation in the sensed quantity (i.e., humidity), offered a change in the capacitance's dielectric constant, alternating the fundamental period of a timer [Figure 8(a) and (b)]; the latter simply controlled the frequency of switching at the tag antenna between two loads, thus shifting the backscattered signal frequency. Tags were deployed in a greenhouse and networked based on simple, frequency-division multiple access. Utilizing the same principles, work in [4] demonstrated soil moisture monitoring across a field with measurement RMS error of 1.9%, while consuming approximately ~100 – 200 μW, at a cost of ~5 Euro per tag; reduced power consumption was achieved by switching off circuit subcomponents when they were not used, while the sensing capacitor inserted in the ground was based on a custom design.

The major disadvantage of coherent communication is the utilization of preamble bits at the packet, a priori known at the reader, for channel estimation.

How about using a plant as a battery and as a sensor? Work in [3] demonstrated the feasibility of implementing backscatter tags, able to measure and transmit (utilizing backscatter FM principles) the electric potential (EP) across two electrodes in the plants' stem, while being solely powered by the plant itself, using another pair of electrodes [Figure 9(a)]. A strong correlation was found between the EP signal, solar irradiation, and the time instants at which the plant was actually watered; thus, the backscattered EP signal indicated when the plant was actually watered (and not just the moisture level in the vicinity of the plant). The tag design consumed only 20 μW, while the plant could offer about 1 μW at noon time; therefore, duty-cycling was needed, allowing the tag to harvest sufficient energy from the plant before backscattering the (information-rich) EP signal.

The aforementioned implementations constitute realizations of backscatter links/networks, able to measure an environmental variable (e.g., humidity, soil moisture, EP of a plant) and transmit the value(s) toward an SDR under a dedicated illuminating carrier. As can be seen from the previous discussion, a computer running appropriate software (to decode the sensor's information from the backscattered signal) is needed along with a separate unit(s) providing the necessary illumination/carrier. Dedicated illumination is not required in ambient setups; work in [5] proposed a backscatter tag that is able to facilitate any capacitive or resistive sensor [Figure 8(c)] that backscatters its information toward any conventional FM radio receiver, including modern smartphones; capacitive soil moisture sensing for agriculture was demonstrated [Figure 9(b)], in more detail in the section "Extensions to Ambient Environments."

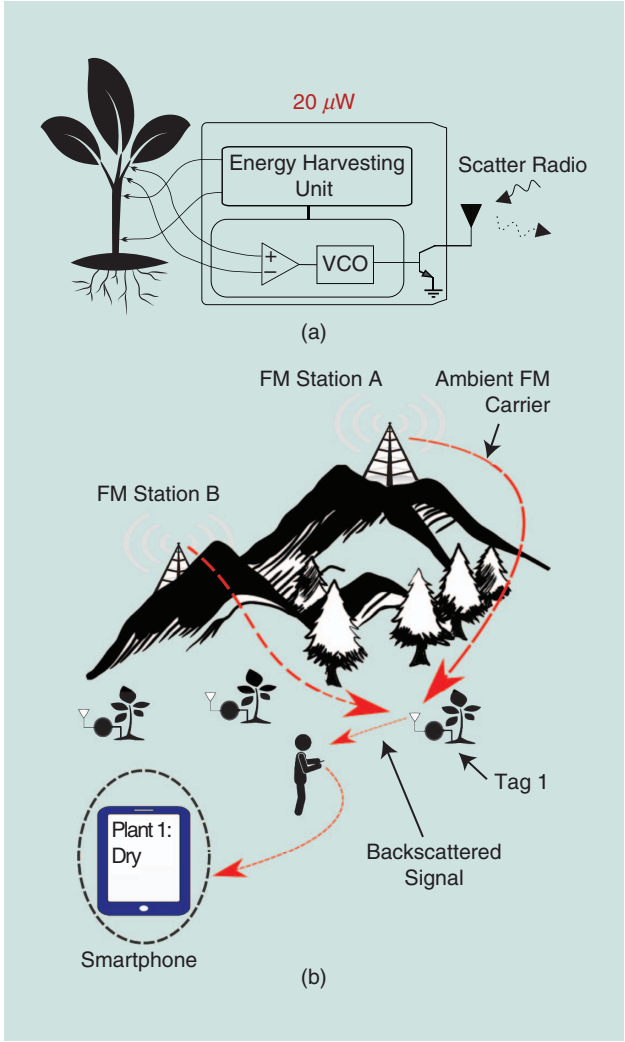

FIGURE 9. Backscatter radio-based IoT technologies could revolutionize environmental sensing and agriculture. (a) The backscattering of the EP of plants with μW consumption, powered by the plant itself [3]. (b) FM remodulation and backscattering from μW environmental sensors [5].

Discussion

Since switching between two antenna loads is the basic tag function for backscattering, a fundamental power consumption limit at each tag emerges: the power cost of a switch! Today's advanced CMOS technology operates at energies on the order of $10^4 - 10^5$ $k_B T_\theta$ per binary switching event using MOSFET switches and von-Neumann architectures, where k_B is the Boltzmann constant and T_θ is the temperature (in Kelvin). It is also noted that the fundamental limit of switching [Guardian Angels, FET Flagship Pilot, Final Report (public version), April 2012, based on information

from R.W. Keyes, *IBM Journal of Research Development* vol. 32, 1988, pp. 24–28, data updated by T. Theis and R. Keyes, IBM Research, 2010] can be calculated from the Boltzmann probability, equal to $3\ln(2)k_BT_\theta \approx 10^{-21}$ J, at room temperature (300° K); assuming switching frequency at the tag between the two loads at 100 kHz, the aforementioned CMOS state-of-the-art energies of $10^4 - 10^5$ k_BT_θ correspond to $(0.5 - 5)\times 10^{-15}$W (fW) power consumption at the tag for room temperature.

The backscatter tag also requires power for the driving signal that controls switching and, of course, the rest of the circuitry needed for sensing (if sensing is also performed); examples of how backscatter radio and sensing can be performed jointly, with minimal additional hardware (e.g., adding a low-power timer), were previously given. Thus, the aforementioned numbers hint that further reduction of tag power consumption at the sub-μW regime is possible in the near future.

In the context of environmental sensing, backscatter networks have been developed for monitoring both environmental humidity and soil moisture.

In terms of signal processing, noncoherent sequence detection with relatively small complexity is challenging for ergodic setups, e.g., when the ambient illuminating signal changes for different backscatter tag bits, or nonergodic setups, when channel conditions (including ambient illuminator's signal) can be assumed constant during tag sequence backscattering; ideas from the work presented in this tutorial may assist. Initial results alongside this distinction, turning ambient modulated (but unknown) signals to an advantage, compared to unmodulated/CW illuminator, can be found in [43].

It is also important to realize that backscattering with simple switching, i.e., without amplifiers or another type of active signal conditioning at the tag, is, in principle, a communication technique at the power-limited regime; thus, typical housekeeping tasks for digital communications, such as CFO estimation, packet and symbol synchronization, dc offset removal, channel estimation, or more advanced tasks, such as successive interference cancellation, should not be idealized or overlooked at small SNRs. Furthermore, realistic assumptions on link budgets and noise at the receiver should be carefully justified.

Finally, it is perhaps important to note that backscatter radio was the first enabling technology for commercial RFID systems, realizing (even though with limited success) exploitation of a remote signal for both communication and power transfer; the same concept can be used to eliminate other parts in a typical receiver chain, e.g., remove the oscillator part in a receiver and exploit the carrier signal from a nearby transmitter (e.g., see the example work in [44]). Shared signaling and electronics open new avenues for realizable, ultralow-power IoT technology of the future. Other promising applications of backscatter radio (relevant to chipless RFID, motion detection, gesture recognition, and indoor localization but not covered in this work) underline the importance of backscatter radio in the years to come.

Acknowledgment

This research is implemented through the Operational Program "Human Resources Development, Education and Lifelong Learning" and is co-financed by the European Union (European Social Fund) and Greek national funds.

Authors

Aggelos Bletsas (aggelos@telecom.tuc.gr) received the diploma degree (with honors) in electrical and computer engineering from the Aristotle University of Thessaloniki, Greece, in 1998, and the S.M. and Ph.D. degrees in media arts and sciences from the Massachusetts Institute of Technology Media Lab, Cambridge in 2001 and 2005, respectively. He currently serves as an associate professor in the School of Electrical and Computer Engineering, Technical University of Crete, Greece. His research interests span the broad area of scalable wireless communications and sensors networking. He was a corecipient of the IEEE Communications Society 2008 Marconi Prize Paper Award in Wireless Communications, and various Best Student Paper Awards, e.g., at both the 2011 and 2017 IEEE International Conference on RFID-Technologies and Applications; the 2015 International Conference on Acoustics, Speech, and Signal Processing; and the 2018 International Conference on Modern Circuits and Systems Technologies.

Panos N. Alevizos (palevizos@isc.tuc.gr) received the diploma, M.Sc., and Ph.D. degrees in electronic and computer engineering from the Technical University of Crete, Greece, in 2012, 2014, and 2017, respectively. His research interests include communication theory and signal processing with an emphasis on backscatter radio and radio-frequency identification. He is a corecipient of the 2015 IEEE International Conference on Acoustics, Speech, and Signal Processing Best Student Paper Award. He has been distinguished as an exemplary reviewer for 2015 by the editorial board of *IEEE Wireless Communications Letters* and for 2017 by the editorial board of *IEEE Transactions on Wireless Communications*.

Georgios Vougioukas (gevougioukas@isc.tuc.gr) received his five-year diploma degree in electrical and computer engineering from the Technical University of Crete, Greece, in 2016, and he is currently pursuing his Ph.D. degree in electrical and computer engineering there. His research interests include methods for ultralow-power wireless communication, signal processing for backscatter communication, energy harvesting, and analog and digital system design and implementation. He was a corecipient of the 2017 IEEE International Conference on RFID Technology and Applications Best Student Paper Award. He has been distinguished as an exemplary reviewer for 2017 by the editorial board of *IEEE Transactions on Wireless Communications*.

References

[1] G. Vannucci, A. Bletsas, and D. Leigh, "A software-defined radio system for backscatter sensor networks," *IEEE Trans. Wireless Commun.*, vol. 7, no. 6, pp. 2170–2179, June 2008.

[2] E. Kampianakis, J. Kimionis, K. Tountas, C. Konstantopoulos, E. Koutroulis, and A. Bletsas, "Wireless environmental sensor networking with analog scatter radio & timer principles," *IEEE Sensors J.*, vol. 14, no. 10, pp. 3365–3376, Oct. 2014.

[3] C. Konstantopoulos, E. Koutroulis, N. Mitianoudis, and A. Bletsas, "Converting a plant to a battery and wireless sensor with scatter radio and ultra-low cost," *IEEE Trans. Instrum. Meas.*, vol. 65, no. 2, pp. 388–398, Feb. 2016.

[4] S. N. Daskalakis, S. D. Assimonis, E. Kampianakis, and A. Bletsas, "Soil moisture scatter radio networking with low power," *IEEE Trans. Microw. Theory Techn.*, vol. 64, no. 7, pp. 2338–2346, July 2016.

[5] G. Vougioukas and A. Bletsas, "24μW 26m range batteryless backscatter sensors with FM remodulation and selection diversity," in *Proc. IEEE Radio Frequency Identification Technology and Applications*, Warsaw, Poland, Sept. 2017, pp. 237–242.

[6] S. J. Thomas and M. S. Reynolds, "A 96 Mbit/sec, 15.5 pJ/bit 16-QAM modulator for UHF backscatter communication," in *Proc. IEEE Radio Frequency Identification Conf.*, Orlando, FL, Apr. 2012, pp. 185–190.

[7] S. Thomas, E. Wheeler, J. Teizer, and M. Reynolds, "Quadrature amplitude modulated backscatter in passive and semipassive UHF RFID systems," *IEEE Trans. Microw. Theory Techn.*, vol. 60, no. 4, pp. 1175–1182, Apr. 2012.

[8] P. Hu, P. Zhang, and D. Ganesan, "Laissez-faire: Fully asymmetric backscatter communication," *ACM SIGCOMM Comput. Commun. Rev.*, vol. 45, no. 4, pp. 255–267, Oct. 2015.

[9] P. N. Alevizos, K. Tountas, and A. Bletsas, "Multistatic scatter radio sensor networks for extended coverage," *IEEE Trans. Wireless Commun.*, to be published.

[10] V. Iyer, V. Talla, B. Kellogg, S. Gollakota, and J. Smith, "Inter-technology backscatter: Towards internet connectivity for implanted devices," in *Proc. ACM Special Interest Group on Data Communications Conf.*, Florianopolis, Brazil, 2016, pp. 356–369.

[11] J. Kimionis, A. Bletsas, and J. N. Sahalos, "Increased range bistatic scatter radio," *IEEE Trans. Commun.*, vol. 62, no. 3, pp. 1091–1104, Mar. 2014.

[12] A. Bletsas, A. G. Dimitriou, and J. Sahalos, "Improving backscatter radio tag efficiency," *IEEE Trans. Microw. Theory Techn.*, vol. 58, no. 6, pp. 1502–1509, June 2010.

[13] J. Kimionis, A. Bletsas, and J. N. Sahalos, "Design and implementation of RFID systems with software defined radio," in *Proc. IEEE European Conf. Antennas and Propagation*, Prague, Czech Republic, Mar. 2012, pp. 3464–3468.

[14] J. Kimionis, A. Bletsas, and J. N. Sahalos, "Bistatic backscatter radio for tag read-range extension," in *Proc. IEEE Radio Frequency Identification Technology and Applications Conf.,* Nice, France, Nov. 2012, pp. 356–361.

[15] J. Kimionis, A. Bletsas, and J. N. Sahalos, "Bistatic backscatter radio for power-limited sensor networks," in *Proc. IEEE Global Communication Conf.*, Atlanta, GA, Dec. 2013, pp. 353–358.

[16] J. D. Griffin and G. D. Durgin, "Gains for RF tags using multiple antennas," *IEEE Trans. Antennas Propag.*, vol. 56, no. 2, pp. 563–570, Feb. 2008.

[17] J. D. Griffin and G. D. Durgin, "Complete link budgets for backscatter-radio and RFID systems," *IEEE Antennas Propag. Mag.*, vol. 51, no. 2, pp. 11–25, Apr. 2009.

[18] V. Liu, A. Parks, V. Talla, S. Gollakota, D. Wetherall, and J. R. Smith, "Ambient backscatter: Wireless communication out of thin air," in *Proc. ACM Special Interest Group on Data Communications Conf.*, Hong Kong, China, 2013, pp. 39–50.

[19] P. N. Alevizos and A. Bletsas, "Noncoherent composite hypothesis testing receivers for extended range bistatic scatter radio WSNs," in *Proc. IEEE Int. Conf. Communications*, London, June 2015, pp. 4448–4453.

[20] P. N. Alevizos, A. Bletsas, and G. N. Karystinos, "Noncoherent short packet detection and decoding for scatter radio sensor networking," *IEEE Trans. Commun.*, vol. 65, no. 5, pp. 2128–2140, May 2017.

[21] P. N. Alevizos, Y. Fountzoulas, G. N. Karystinos, and A. Bletsas, "Noncoherent sequence detection of orthogonally modulated signals in flat fading with log-linear complexity," in *Proc. IEEE Int. Conf. Acoustics Speech and Signal Processing*, Brisbane, Australia, Apr. 2015, pp. 2974–2978.

[22] P. N. Alevizos, Y. Fountzoulas, G. N. Karystinos, and A. Bletsas, "Log-linear-complexity GLRT-optimal noncoherent sequence detection for orthogonal and RFID-oriented modulations," *IEEE Trans. Commun.*, vol. 64, no. 4, pp. 1600–1612, Apr. 2016.

[23] N. Fasarakis-Hilliard, P. N. Alevizos, and A. Bletsas, "Coherent detection and channel coding for bistatic scatter radio sensor networking," *IEEE Trans. Commun.*, vol. 63, pp. 1798–1810, May 2015.

[24] P. N. Alevizos, N. Fasarakis-Hilliard, K. Tountas, N. Agadakos, N. Kargas, and A. Bletsas, "Channel coding for increased range bistatic backscatter radio: Experimental results," in *Proc. IEEE Radio Frequency Identification Technology and Applications Conf.*, Tampere, Finland, Sept. 2014, pp. 38–43.

[25] N. Fasarakis-Hilliard, P. N. Alevizos, and A. Bletsas, "Coherent detection and channel coding for bistatic scatter radio sensor networking," in *Proc. IEEE Int. Conf. Communications*, June 2015, pp. 4895–4900.

[26] N. Kargas, F. Mavromatis, and A. Bletsas, "Fully-coherent reader with commodity SDR for Gen2 FM0 and computational RFID," *IEEE Wireless Commun. Lett.*, vol. 4, no. 6, pp. 617–620, Dec. 2015.

[27] J. F. Ensworth and M. S. Reynolds, "Every smart phone is a backscatter reader: Modulated backscatter compatibility with Bluetooth 4.0 Low Energy (BLE) devices," in *Proc. IEEE Radio Frequency Identification Conf.*, San Diego, CA, Apr. 2015, pp. 78–85.

[28] G. Vougioukas, S. N. Daskalakis, and A. Bletsas, "Could battery-less scatter radio tags achieve 270-meter range?," in *Proc. IEEE Wireless Power Transfer Conf.*, Aveiro, Portugal, May 2016, pp. 1–3.

[29] D. Darsena, G. Gelli, and F. Verde, "Modeling and performance analysis of wireless networks with ambient backscatter devices," *IEEE Trans. Commun.*, vol. 65, no. 4, pp. 1797–1814, Apr. 2017.

[30] J. Qian, F. Gao, G. Wang, S. Jin, and H. Zhu, "Noncoherent detections for ambient backscatter system," *IEEE Trans. Wireless Commun.*, vol. 16, no. 3, pp. 1412–1422, Mar. 2017.

[31] G. Wang, F. Gao, R. Fan, and C. Tellambura, "Ambient backscatter communication systems: Detection and performance analysis," *IEEE Trans. Commun.*, vol. 64, no. 11, pp. 4836–4846, Nov. 2016.

[32] J. Qian, F. Gao, G. Wang, S. Jin, and H. Zhu, "Semi-coherent detection and performance analysis for ambient backscatter system," *IEEE Trans. Commun.*, vol. 65, no. 12, pp. 5266–5279, Dec. 2017.

[33] G. Yang, Y. Liang, R. Zhang, and Y. Pei. (2017). Modulation in the air: Backscatter communication over ambient OFDM carrier. [Online]. Available: http://arxiv.org/abs/1704.02245

[34] D. T. Hoang, D. Niyato, P. Wang, D. I. Kim, and Z. Han, "Ambient backscatter: A new approach to improve network performance for RF-powered cognitive radio networks," *IEEE Trans. Commun.*, vol. 65, no. 9, pp. 3659–3674, Sept. 2017.

[35] K. Han and K. Huang, "Wirelessly powered backscatter communication networks: Modeling, coverage and capacity," *IEEE Trans. Wireless Commun.*, vol. 16, no. 4, pp. 2548–2561, Apr. 2017.

[36] N. V. Huynh, D. T. Hoang, X. Lu, D. Niyato, P. Wang, and D. I. Kim, "Ambient backscatter communications: A contemporary survey," arXiv Preprint, arXiv: 1712.04804, Dec. 2017.

[37] A. N. Parks, A. Liu, S. Gollakota, and J. R. Smith, "Turbocharging ambient backscatter communication," in *Proc. ACM Special Interest Group Data Communications Conf.*, Chicago, IL, 2014, pp. 619–630.

[38] A. Wang, V. Iyer, V. Talla, J. R. Smith, and S. Gollakota, "FM backscatter: Enabling connected cities and smart fabrics," in *Proc. USENIX Symp. Networked Systems Design and Implementation Conf.*, Boston, MA, Mar. 2017, pp. 243–258.

[39] S. N. Daskalakis, J. Kimionis, A. Collado, G. Goussetis, M. M. Tentzeris, and A. Georgiadis, "Ambient backscatterers using FM broadcasting for low cost and low power wireless applications," *IEEE Trans. Microw. Theory Techn.*, vol. PP, no. 99, pp. 1–12, 2017.

[40] B. Kellogg, A. Parks, S. Gollakota, J. R. Smith, and D. Wetherall, "Wi-Fi backscatter: Internet connectivity for rf-powered devices," in *Proc. ACM Special Interest Group Data Communications Conf.*, Chicago, IL, 2014, pp. 607–618.

[41] D. Bharadia, K. R. Joshi, M. Kotaru, and S. Katti, "Backfi: High throughput WiFi backscatter," in *Proc. ACM Special Interest Group Data Communications Conf.*, London, 2015, pp. 283–296.

[42] P. Zhang, D. Bharadia, K. Joshi, and S. Katti, "Hitchhike: Practical backscatter using commodity WiFi," in *Proc. ACM Conf. Embedded Networked Sensing Systems*, 2016, pp. 259–271.

[43] G. Vougioukas and A. Bletsas, "Switching frequency techniques for universal ambient backscatter networking," submitted for publication.

[44] A. Varshney, O. Harms, C. P. Penichet, C. Rohner, F. Hermans, and T. Voigt, "Lorea: A backscatter architecture that achieves a long communication range," in *Proc. ACM Conf. Embedded Networked Sensing Systems*, Delft, The Netherlands, Nov. 2017, pp. 50:1–50:2.

SP